ACS APPLIED MATERIALS & INTERFACES

Research Article

www.acsami.org

Adsorption-Induced Crystallization of U-Rich Nanocrystals on Nano-$Mg(OH)_2$ and the Aqueous Uranyl Enrichment

Zhi Chen,[†,‡] Zanyong Zhuang,*[,†] Qing Cao,[†] Xiaohong Pan,[†,‡] Xiong Guan,[‡] and Zhang Lin*[,†]

[†]State Key Laboratory of Structural Chemistry, Fujian Institute of Research on the Structure of Matter, Chinese Academy of Sciences, Fuzhou, Fujian, 350002, P. R. China

[‡]Key Lab of Biopesticide and Chemical Biology, Fujian Agriculture and Forestry University, Ministry of Education, Fuzhou, Fujian 350002, P. R. China

Supporting Information

ABSTRACT: The mechanism of the interaction between nano-$Mg(OH)_2$ adsorbent and uranyl in water was studied. At trace levels, the uranyl is adsorbed as a monolayer on nano-$Mg(OH)_2$, and occupied a small proportion of the adsorption sites. As the uranyl concentration crosses over a threshold, continuous increase of adsorption capacity takes place. It indicates that, by taking the pre-adsorbed uranyl as the nucleation centers, the additional uranyl crystallizes and forms U-rich nanocrystals well-scattered on the surface of nano-$Mg(OH)_2$. A strategy of inducing fast crystal growth of nano-$Mg(OH)_2$ to micrometer-sized $Na_2Mg(CO_3)_2$ enables the desorption and enrichment of uranyl. The recycling and reuse of nano-$Mg(OH)_2$ can be achieved simultaneously. The finding in this work provides fundamental understanding of the efficient usage of nano-$Mg(OH)_2$ in practical applications.

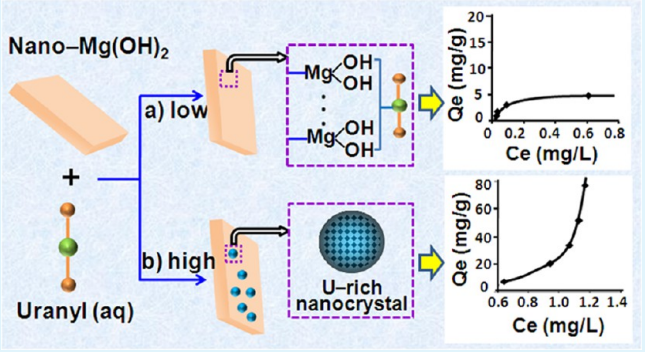

KEYWORDS: *nano-$Mg(OH)_2$, uranyl, adsorption, mechanism, crystallization, enrichment*

INTRODUCTION

The burgeoning demand for nuclear energy as a low-carbon energy source has raised serious concerns about the environmental uranium contamination on one hand and the limited reserves of terrestrial uranium on the other.[1] To both issues, the key lies in extracting uranium from nonconventional resources such as industrial waste water and sea/lake water containing extremely high levels of dissolved uranium.[1−4]

So far, the sorption-based strategy is considered to be one of the most promising methods for uranium collection. Although synthesis of adsorbents with high adsorption capacity has been achieved, comprehensive studies on the underlying adsorption mechanism are conducive to the design and applications of novel adsorbents. For instance, layered metal sulfide (KMS-1) showed a remarkably high exchange capacity toward UO_2^{2+} ions based on an ion-exchange mechanism (a bulk property of the materials).[5] In some cases, the superb adsorptive properties arose from chemical reactions between the adsorbents and the target, e.g., $Mg(OH)_2 + Tb^{3+} \rightarrow Tb(OH)_3$.[6] For nanomaterials such as metal silicate nanotubes, their large surface area and abundant active sites played an important role in their efficient extraction of uranyl ions and other matters in water.[7]

Sometimes, the adsorption mechanism and kinetics could be sensitive to experiment conditions such as pH, temperature, or concentrations of the adsorbates. For example, Farley et al. found that the sorption of cations on metal oxides underwent continuous surface reactions and precipitation, the occurrence of which was dependent on adsorbates concentration. This process was further described by a so-called surface precipitation model,[8] and the mechanism also controls the uptake of uranium and trace elements by pyrite (FeS_2) suspensions.[9] Recently, we demonstrated that nano-$Mg(OH)_2$, as a nontoxic and environmentally friendly material,[10−13] possesses higher adsorption affinity (denoted as b value) toward uranyl than many other existing adsorbents, and exhibits good extraction efficiency and selectivity toward trace uranium (ppb) in water.[14] As indicated by the adsorption isotherm that followed the Langmuir mechanism, the trace uranyl was adsorbed as a monolayer onto the surface of nano-$Mg(OH)_2$.[14] However, only a small proportion of the adsorption sites of nano-$Mg(OH)_2$ were occupied even at the saturation point. These clues above trigger us to compare the interaction between nano-$Mg(OH)_2$ and uranyl under low and high concentration, the results of which can shed lights to the prediction and use of $Mg(OH)_2$ adsorbents.

In this work, the adsorption of uranyl on nano-$Mg(OH)_2$ in the low (0.5−10 mg/L) and high (10−100 mg/L) concentration ranges was found to follow distinct mechanisms. Different from the monolayer adsorption behavior at trace levels, crystallization of U-rich nanocrystals on nano-$Mg(OH)_2$

Received: November 23, 2013
Accepted: December 26, 2013
Published: December 26, 2013

   dx.doi.org/10.1021/am405306j | ACS Appl. Mater. Interfaces 2014, 6, 1301−1305

surface at high concentrations drastically increased adsorption capacity, the underlying mechanism of which was discussed. Previously, we developed a strategy of using CO_2 mineralizer to enrich Cr^{VI} and recycle nano-$Mg(OH)_2$ during Cr^{VI} treatment.[15,16] By inducing fast crystal growth of nano-$Mg(OH)_2$ particles, micrometer-sized $Na_2Mg(CO_3)_2$ was proposed in this work to desorb and enrich uranyl, and to recycle nano-$Mg(OH)_2$ and mineralizer $NaHCO_3$. This study would further our understanding of the highly efficient and environmentally friendly $Mg(OH)_2$ nanoadsorbent in the aqueous extraction of uranyl and other matters in practical application processes.

MATERIALS AND METHODS

Materials and Chemicals. All chemicals were of reagent grade, and all solutions were prepared using deionized water. MgO and $NaHCO_3$ were purchased from National Chemical Corporation Ltd. of China. Uranyl acetate dihydrate was acquired from Aladdin Reagent (Shanghai) Co., Ltd. Stock solution of U(VI) (1000 mg/L) was prepared by dissolving $UO_2(AC)_2{\cdot}2H_2O$ into deionized water.

Adsorption Kinetics. Batch adsorption experiments were conducted by equilibrating 0.2 g MgO in 200 mL uranyl solution of 40 mg/L. At pre-determined time intervals, a fraction of adsorbents were centrifuged at the speed of 8000 rpm for 3 min. The concentration of uranyl in the supernatant was analyzed by an ultraviolet pulse trace uranium analyzer (WGJ-III). In addition, the precipitate was collected and dried to be analyzed by X-ray diffraction (XRD), transmission electron microscopy (TEM), and scanning electron microscope (SEM).

Adsorption Isotherms. A fixed amount of 0.04 g of MgO was added into 40 mL of uranyl solution of different concentrations ranging from 0.5 to 100 mg/L. A fraction of the mixture was centrifuged after the adsorption reached equilibrium. The supernatant and the precipitate were analyzed using the same techniques as those used in the adsorption kinetics study.

Phase Identification of Uranium. To identify the phase of U(VI) adsorbed on the adsorbent, we equilibrated 0.2 g of MgO in 10 mL of uranyl solution of 4000 mg/L for 30 min. The precipitate was separated, dried, and analyzed by the XRD and TEM.

Enrichment of Uranyl and Recycling of Adsorbent. U(VI)-loaded samples of ~0.5 g were treated at 150 °C for 20 h using $NaHCO_3$. After this treatment, the samples were heated at 700 °C for 3 h to produce MgO. This white solid product was then dissolved in distilled water for the regeneration of $Mg(OH)_2$. After centrifugation at 8000 rpm for 5 min, the $Mg(OH)_2$ sample was put back into the uranyl-containing solution for the next adsorption cycle. During this process, the adsorbent was characterized by XRD and SEM.

Characterization. XRD data were collected on a PANalyticalX'-Pert PRO diffractometer with Cu Kα radiation (40 kV, 40 mA) in the continuous scanning mode. The 2θ scanning range was from 5 to 85° in steps of 0.008° with a collection time of 50 s per step. The morphologies and sizes of the solids were characterized with a JEOL-6700F SEM and a JEOL JEM2010 TEM coupled with an energy-dispersive X-ray spectroscopy (Oxford) system operated at 200 kV.

RESULTS AND DISCUSSION

Preparation of Nano-$Mg(OH)_2$ Adsorbent. The Mg-$(OH)_2$ nanoadsorbents were prepared by the hydration of MgO in as-prepared uranyl solution under continuous stirring. Figure 1 shows the typical XRD pattern, SEM and TEM images of the as-synthesized $Mg(OH)_2$. The XRD data can be indexed by hexagonal $Mg(OH)_2$ with a calculated average size of 18.8 ±1.3 nm in [001] direction and 29.5 ± 3.1 nm in [101] direction. In line with the XRD result, SEM and TEM images further show that the $Mg(OH)_2$ are single-crystal nanoplatelets with a thickness of roughly 20 nm in [001] direction. The BET

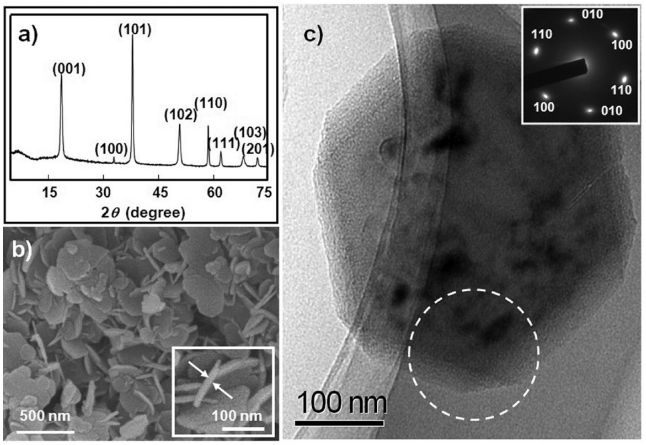

Figure 1. Typical (a) XRD pattern, (b) SEM image (inset showing enlarged details), and (c) TEM image of as-synthesized $Mg(OH)_2$ nanoplatelets by the hydration of MgO. Selected area electron diffraction pattern (inset of c) of nanoplatelets well-defined spots in 6-fold symmetry with z axis at [001] of $Mg(OH)_2$.

measurements give a specific surface area of 50.1 m^2/g for the $Mg(OH)_2$ nanoplatelet.

Isotherm for Uranyl Adsorption on Nano-$Mg(OH)_2$. To assess the adsorption capacity and affinity of nano-$Mg(OH)_2$ towards uranyl acetate, experimental equilibrium data (Q_e vs. C_e) were collected for uranyl acetate adsorption by 1.45 g/L $Mg(OH)_2$ over the initial concentration range of 0.5−100 mg/L. As shown in Figure 2a, when the initial concentration is lower than ~10 mg/L, Q_e maximizes at 6.3 mg/g. Adsorption kinetics (see the Supporting information, part I, Table S1) indicates that the trace uranyl is adsorbed as a monolayer onto the surface of nano-$Mg(OH)_2$. At an initial concentration higher than 10 mg/L, a much higher Q_e can be seen. The Q_e value increases with C_e. For example, the Q_e value of 73 mg/g corresponds to an initial concentration of 100 mg/L, which exemplifies a much higher adsorption capacity for uranyl at high concentrations. In Figure 2b, the time-dependent curve of uranyl acetate uptake proves the adsorption rate and high efficiency of nano-$Mg(OH)_2$ toward high concentrations of uranyl acetate. More than 96% uptake occurred in the first 30 min when 0.2 g of MgO was added into 200 mL of uranyl acetate solution of 40 mg/L. The results indicates that nano-$Mg(OH)_2$ has higher removal efficiency toward high-concentration uranyl, in addition to a high capacity.

To investigate the rate-limiting step, the adsorption data were further fitted by pseudo-first-order[17] and pseudo-second-order[18] equations, wherein the latter fit our experimental data better. Table 1 summarizes the kinetic parameters obtained by linear regression according to the pseudo-second-order equation, and the fitting results are showed in Figure 2c. The result suggested that the rate-limiting step might be chemisorption.[19−21] Moreover, the value of $t_{1/2}$ decreases gradually as the initial uranyl concentration increases from 20 to 100 mg/L. The decrease of $t_{1/2}$ implies that the uranyl could be removed more quickly by nano-$Mg(OH)_2$ from solutions and approach the half-equilibrium state in high concentrations.

Phase of Uranium Loaded on Nano-$Mg(OH)_2$. Figure 3 shows the XRD patterns of $Mg(OH)_2$ sample after the treatment with 10−100 mg/L uranyl solutions. There are no uranium diffraction peaks after the treatment with 10−40 mg/L uranyl solution. The amount of adsorbed U(VI) may be too

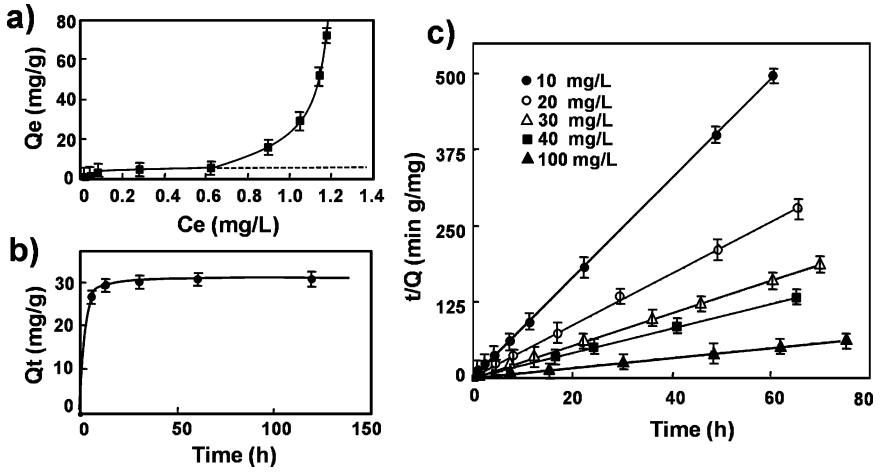

Figure 2. (a) Isotherm for uranyl adsorption on nano-$Mg(OH)_2$; (b) effect of contact time on the adsorption of uranyl (40 mg/L); (c) pseudo-second-order fitting and isotherm of different concentrations.

Table 1. Kinetic Parameters for the Adsorption of Concentrated Uranyl Fitted by the Pseudo-Second-Order Equation

C_0 (mg/L)	R^2	Q_e (mg/g)	k (g mg^{-1} min^{-1})	h (mg g^{-1} min^{-1})	$t_{1/2}$ (min)
10	0.9999	6.72	7.766×10^{-2}	3.50	1.92
20	0.9994	13.37	6.858×10^{-3}	1.23	10.91
30	0.9999	20.41	5.268×10^{-3}	2.19	9.30
40	0.9999	26.81	5.431×10^{-3}	3.90	6.87
100	0.9999	68.03	5.556×10^{-3}	25.71	2.65

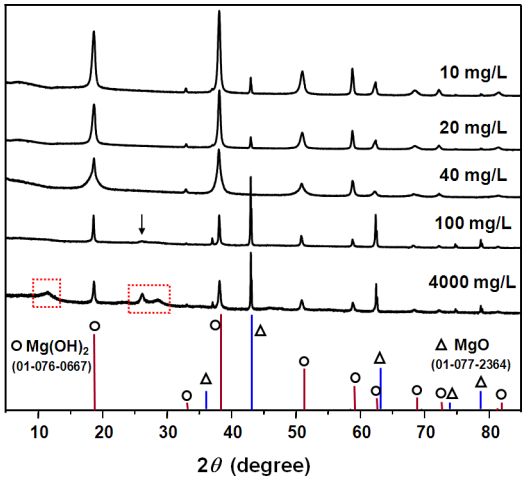

Figure 3. Typical XRD patterns for dried $Mg(OH)_2$ sorption samples reacted with different concentrations of U(VI).

low to be detected by XRD. However, when the initially uranyl concentration is up to 100 mg/L, compared with the XRD pattern of primary $Mg(OH)_2$ in Figure 1a, a weak and broaden diffraction peak ~26° can be observed, which cannot be assigned to the diffraction features of MgO or $Mg(OH)_2$. Because 6% uranium was found in sample by ICP analysis, this newly observed diffraction peak ~26° could be a uranium-rich phase. To verify this, we further treated nano-$Mg(OH)_2$ by uranyl acetate as high as 4000 mg/L for 30 min. As shown in Figure 3, the intensity of diffraction peaked around ~26° is enhanced. It confirms the newly observed diffraction peak to be a uranium-rich phase. Moreover, a calculation based on the broadened diffraction peak by using Scherrer equation suggests the small size of new uranium compounds were formed. An average size of 4 nm can be obtained by the Scherrer equation, which indicates that the fast adsorbed uranyl transformed into U-rich nanocrystals.

HRTEM was used to confirm the size, morphology, and crystal structure of newly generated uranyl phase. Figure 4a

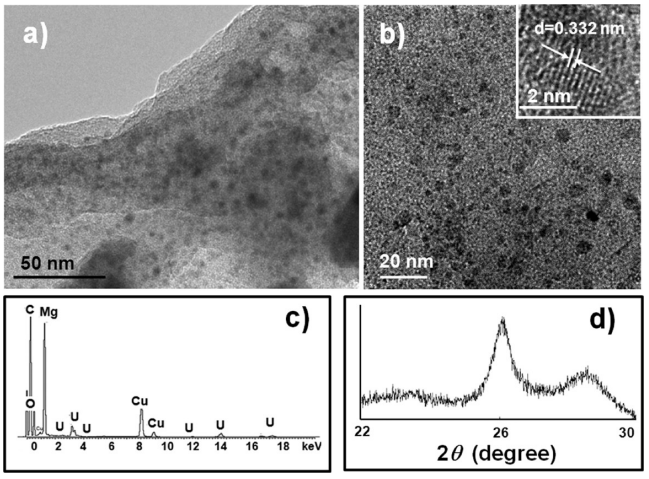

Figure 4. (a, b) HRTEM images of nano-$Mg(OH)_2$ with uranyl adsorption; (c) EDS analysis of sample a; (d) enlarged XRD pattern (22–30°) of $Mg(OH)_2$ sample after reacting with 4000 mg/L uranyl.

shows the HRTEM image of nano-$Mg(OH)_2$ after the treatment by 4000 mg/L uranyl adsorption. On the surface of $Mg(OH)_2$ are adsorbed large amounts of nanoparticles (Figure 4b) with particle size ranging from 3 to 6 nm. This result is in line with the XRD analysis. Further analysis of the sample shows that the lattice spacing of the nanocrystals measured d = 0.332 nm. This is identical to the value of ~26.8° calculated from the XRD pattern by the Bragg equation. As shown in Figure 4c, the Mg, U, and O signals in the EDS analysis further confirm that new nano-uranium compounds were formed on the surface of $Mg(OH)_2$ in the adsorption process.

Proposed Adsorption Mechanism of Uranyl on Nano-$Mg(OH)_2$. The isotherms shown in Figure 2a can be described by three different domains according to the isotherm shape.

dx.doi.org/10.1021/am405306j | ACS Appl. Mater. Interfaces 2014, 6, 1301–1305

Similar phenomenon can be found in earlier studies such as the sorption of cations on metal oxides and the uptake of uranium and trace elements in pyrite (FeS_2) suspensions.[8,9] In their studies, a surface precipitation model was proposed to describe the increasing-type sorption isotherms at high concentrations. However, details about this process are still poorly understood.

As shown in Figure 5, the uptake of trace uranium follows the Langmuir isotherm at low concentrations, which implies

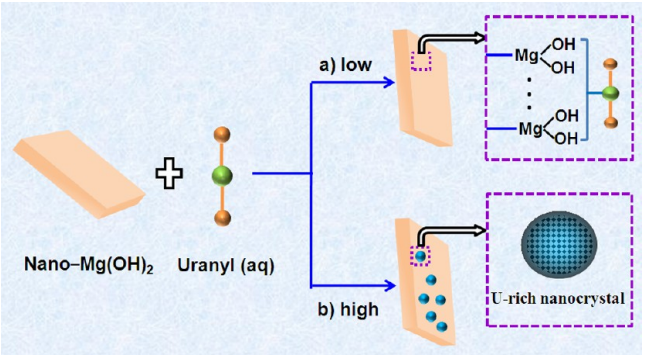

Figure 5. Two adsorption mechanisms of uranyl on nano-$Mg(OH)_2$ at low and high concentrations.

that uranyl was adsorbed to the monolayer surface. With the increase in the concentration, the adsorption reached saturation. It was determined that the surface hydroxide density of $Mg(OH)_2$ is around 11.7 sites per nm^2. Combining with the specific surface area from BET measurement and the adsorption capacity (Q^0 in the Supporting Information, Table S1), it can be calculated that 1 out of every 19 hydroxide sites was occupied by each uranyl complex in an ideal surface model. In other words, it suggests that most of the sorption sites of nano-$Mg(OH)_2$ remain unconnected to uranyl even at saturated adsorption. Interestingly, the excess uranyls have not attached onto the residual sorption sites of nano-$Mg(OH)_2$. With the further increase in the concentration, a sudden increase in the adsorption capacity of uranyl was found. This is because uranium-containing particles of several nanometers were formed on the surface of nano-$Mg(OH)_2$. HRTEM analysis indicates that these nanoparticles were well-scattered onto the surface of nano-$Mg(OH)_2$, which implies these newly formed uranyl nanoparticles should not have nucleated and crystallized in solution. In solution nucleation without organic additive, nanoparticles are normally highly aggregated,[22,23] before attaching onto the surface of $Mg(OH)_2$.

On the basis of the above analysis, we propose that the fast uptake of uranyl at high concentrations to follow a two-step surface precipitation model. First, a monolayer of hydrolyzed uranyl forms onto $Mg(OH)_2$, which allows further mass transfer of sorbate or sorbent metal to the adsorbent. Second, crystalline forms of these compounds appear as a uranyl-rich phase, taking the preadsorption surface sites as nucleation centers. The $t_{1/2}$ analysis suggests that the crystallization reaction accelerated with the increasing concentration of uranyl. In other words, the adsorption kinetics of uranyl on $Mg(OH)_2$ depend on the uranyl concentration, and an effectively high sorption capacity was induced by the surface precipitation and crystalline model.

Strategy for Enrichment of Uranyl and Recycling of Adsorbent. It is a critical factor to desorb and enrich uranyl from the adsorbents. Previously, in the treatment of Cr^{VI}-containing nanowastes, we reported that transforming nano-$Mg(OH)_2$ into bulk materials using $NaHCO_3$ as a mineralizer could facilitate the release of the adsorbed Cr^{VI} into solution.[24] This hydrothermal strategy was tested on the U-loaded $Mg(OH)_2$. As shown in panels a and b in Figure 6, nano-

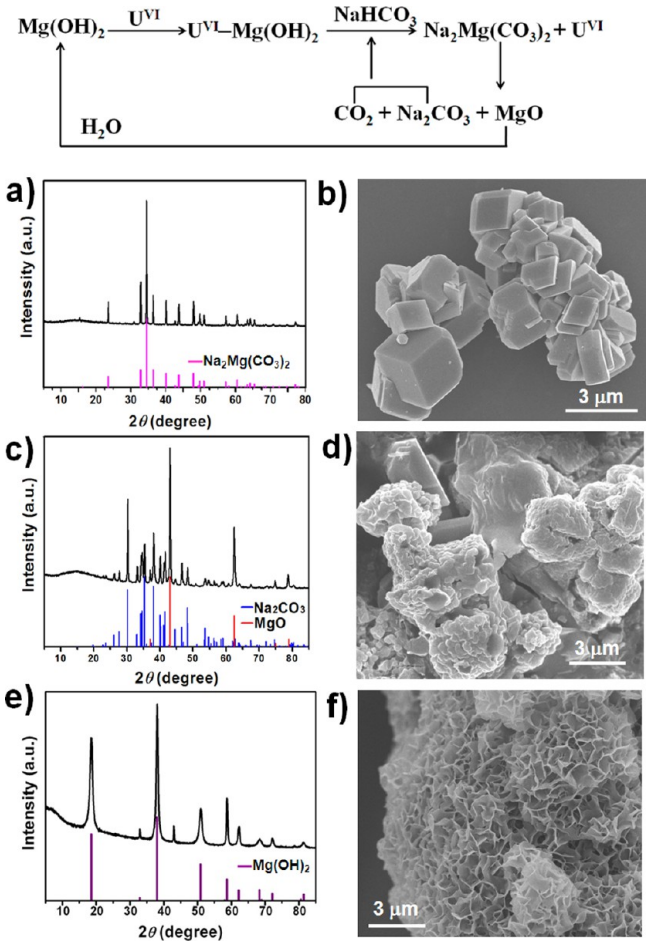

Figure 6. XRD patterns and typical SEM images of (a, b) $Mg(OH)_2$-U(VI) loaden product after treating with $NaHCO_3$ mineralizer; (c, d) calcined sample after phase transformation; (e, f) the regeneration of $Mg(OH)_2$.

$Mg(OH)_2$ after hydrothermally treated by $NaHCO_3$ (150 °C for 20 h) transformed into bulk $Na_2Mg(CO_3)_2$ with size up to several micrometers. It indicated that more than 96% uranium nanocrystals can be removed from the surface of adsorbent, and enrichment multiples of uranyl can reach over 53 (see the Supporting Information, part II, Table S2).

To reduce the cost and environmental impact, the recycling and reuse of nano-$Mg(OH)_2$ was further studied. First, bulk $Na_2Mg(CO_3)_2$ crystals were heated at 700 °C for 3 h. The XRD pattern and SEM image (Figure 6c, d) confirm that $Na_2Mg(CO_3)_2$ decomposed into MgO and Na_2CO_3. Given that the MgO and Na_2CO_3 had different solubility in water, the calcined sample was dissolved in distilled water. In this hydration process, MgO becomes nano-$Mg(OH)_2$ (Figure 6e, f), wherein the regenerated $Mg(OH)_2$ and Na_2CO_3 can be separated by filtration. After three cycles (see the Supporting Information, Table S2), the regenerated $Mg(OH)_2$ nano-adsorbent sustained excellent adsorption ability. The recycling and reuse of nano-$Mg(OH)_2$ follows the reaction route in

dx.doi.org/10.1021/am405306j | ACS Appl. Mater. Interfaces 2014, 6, 1301−1305

Figure 6. The schematic for the uptake and preconcentration of aqueous uranyl is shown in the Supporting Information (part III, Figure S1).

CONCLUSION

Nano-$Mg(OH)_2$, as a nontoxic, inexpensive and environmentally friendly material, had distinct adsorption mechanisms at low and high concentrations of uranyl. At trace levels, nano-$Mg(OH)_2$ possesses higher adsorption affinity (b value) toward uranyl and exhibits good extraction efficiency and selectivity toward trace uranium (ppb) in water. At high concentrations, taking the pre-adsorbed uranyl as nucleation centers, the additional uranyls crystallize and form U-rich nanocrystals, resulting in a high capacity. These characters make nano-$Mg(OH)_2$ to be a promising adsorbent for treating uranium-containing wastewater of both low and high concentrations. Combined with a strategy involving fast crystal growth of nano-$Mg(OH)_2$ particles, the uptake and enrichment of uranyls, as well as the recycling and reuse of nano-$Mg(OH)_2$ adsorbent can be achieved simultaneously. Considering that the sea and saline water in nature are rich in magnesium source, an *in situ* precipitation of nano-$Mg(OH)_2$ could help to reduce the cost. The finding in this work provides fundamental understanding of the efficient usage of nano-$Mg(OH)_2$ in practical applications of heavy metals harvesting.

ASSOCIATED CONTENT

Supporting Information

Additional figure and tables depicting the data in: (i) Langmuir constants associated with adsorption isotherms for uranyl adsorption on nano-$Mg(OH)_2$, (ii) batch experiments of uranyl adsorption, desorption and enrichment, and (iii) the scheme of the uptake and preconcentration of aqueous uranyl. This material is available free of charge via the Internet at http://pubs.acs.org.

AUTHOR INFORMATION

Corresponding Authors

*E-mail: zlin@fjirsm.ac.cn. Tel. & Fax: (+086)591-83705474.
*E-mail: zyzhuang@fjirsm.ac.cn.

Notes

The authors declare no competing financial interest.

ACKNOWLEDGMENTS

This work was supported by the National Basic Research Program of China (2010CB933501, 2013CB934302), the Outstanding Youth Fund (21125730), the National Science Foundation Grant (21273237), the Knowledge Innovation Program (KJCX2-YW-N50, KJCX2-EW-J02), and "Strategic Priority Research Program" (XDA09030203) of the Chinese Academy of Sciences, the Fujian Science Foundation Grant (2012J05035).

REFERENCES

(1) Johnson, B. E.; Santschi, P. H.; Chuang, C. Y.; Otosaka, S.; Addleman, R. S.; Douglas, M.; Rutledge, R. D.; Chouyyok, W.; Davidson, J. D.; Fryxell, G. E.; Schwantes, J. M. *Environ. Sci. Technol.* **2012**, *46*, 11251−11258.
(2) Davies, R. V.; Kennedy, J.; Hill, K. M.; McIlroy, R. W.; Spence, R. *Nature* **1964**, *203*, 1110−1115.
(3) Milja, T. E.; Prathish, K. P.; Prasada Rao, T. *J. Hazard. Mater.* **2011**, *188*, 384−390.
(4) Tian, G.; Teat, S. J.; Zhang, Z.; Rao, L. *Dalton Trans.* **2012**, *41*, 11579−11586.
(5) Manos, M. J.; Kanatzidis, M. G. *J. Am. Chem. Soc.* **2012**, *134*, 16441−16446.
(6) Li, C.; Zhuang, Z.; Huang, F.; Wu, Z.; Hong, Y.; Lin, Z. *ACS Appl. Mater. Interfaces* **2013**, *5*, 9719−9725.
(7) Qu, J.; Li, W.; Cao, C. Y.; Yin, X. J.; Zhao, L.; Bai, J.; Qin, Z.; Song, W. G. *J. Mater. Chem.* **2012**, *22*, 17222−17226.
(8) Farley, K. J.; Dzombak, D. A.; Morel, F. M. M. *J. Colloid Interface Sci.* **1985**, *106*, 226−242.
(9) Descostes, M.; Schlegel, M. L.; Eglizaud, N.; Descamps, F.; Miserque, F.; Simoni, E. *Geochim. Cosmochim. Ac.* **2010**, *74*, 1551−1562.
(10) Alavi, M. A.; Morsali, A. *Ultrason. Sonochem.* **2010**, *17*, 441−446.
(11) Wu, J.; Yan, H.; Zhang, X.; Wei, L.; Liu, X.; Xu, B. *J. Colloid Interface Sci.* **2008**, *324*, 167−171.
(12) Pan, X. H.; Wang, Y. H.; Chen, Z.; Pan, D. M.; Cheng, Y. J.; Liu, Z. J.; Lin, Z.; Guan, X. *ACS Appl. Mater. Interfaces* **2013**, *5*, 1137−1142.
(13) Wang, Y. J.; Chen, J. P.; Lu, L. L.; Lin, Z. *ACS Appl. Mater. Interfaces* **2013**, *5*, 7698−7703.
(14) Cao, Q.; Huang, F.; Zhuang, Z.; Lin, Z. *Nanoscale* **2012**, *4*, 2423−2430.
(15) Liu, W.; Huang, F.; Wang, Y.; Zou, T.; Zheng, J.; Lin, Z. *Environ. Sci. Technol.* **2011**, *45*, 1955−1961.
(16) Lv, X.; Chen, Z.; Wang, Y.; Huang, F.; Lin, Z. *ACS Appl. Mater. Interfaces* **2013**, *5*, 11271−11275.
(17) Lagergren, S. *K. Sven. Vetenskapsakad. Handl.* **1898**, *24*, 1−39.
(18) Ho, Y. S.; McKay, G. *Process Saf. Environ.* **1998**, *76*, 332−340.
(19) Liu, Y. *Colloids Surf., A* **2008**, *320*, 275−278.
(20) Pan, J. M.; Yao, H.; Xu, L. C.; Ou, H. X.; Huo, P. W.; Li, X. X.; Yan, Y. S. *J. Phys. Chem. C* **2011**, *115*, 5440−5449.
(21) Wang, Z.; Xiang, B.; Cheng, R.; Li, Y. *J. Hazard. Mater.* **2010**, *183*, 224−232.
(22) Zhuang, Z.; Xu, X.; Wang, Y.; Wang, Y.; Huang, F.; Lin, Z. *J. Hazard. Mater.* **2012**, *211-212*, 414−419.
(23) Zhuang, Z.; Huang, F.; Lin, Z.; Zhang, H. *J. Am. Chem. Soc.* **2012**, *134*, 16228−16234.
(24) Liu, W.; Huang, F.; Liao, Y.; Zhang, J.; Ren, G.; Zhuang, Z.; Zhen, J.; Lin, Z.; Wang, C. *Angew. Chem., Int. Ed.* **2008**, *47*, 5619−5622.